Elasticity of Polymer Networks

ARTICLE *in* MACROMOLECULES · AUGUST 2002

Impact Factor: 5.8 · DOI: 10.1021/ma0203849

2 AUTHORS, INCLUDING:

S. Panyukov
Russian Academy of Sciences
151 PUBLICATIONS **2,141** CITATIONS

Elasticity of Polymer Networks

Michael Rubinstein*

Department of Chemistry, University of North Carolina, Chapel Hill, North Carolina 27599-3290

Sergei Panyukov

P. N. Lebedev Physics Institute, Russian Academy of Sciences, Moscow, Russia 117924

Received March 13, 2002

ABSTRACT: We develop and solve a new molecular model for nonlinear elasticity of entangled polymer networks. This model combines and generalizes several succeseful ideas introduced over the years in the field of the rubber elasticity. The topological constraints imposed by the neighboring network chains on a given network are represented by the confining potential that changes upon network deformation. This topological potential restricts fluctuations of the network chain to the nonaffinely deformed confining tube. Network chains are allowed to fluctuate and redistribute their length along the contour of their confining tubes. The dependence of the stress σ on the elongation coefficient λ for the uniaxially deformed network is usially represented in the form of the Mooney stress, $f^*(1/\lambda) = \sigma/(\lambda - 1/\lambda^2)$. We find a simple expression for the Mooney stress, $f^*(1/\lambda) = G_c + G_e/(0.74\lambda + 0.61\lambda^{-1/2} - 0.35)$, where G_c and G_e are phantom and entangled network moduli. This allows one to analyze the experimental data in the form of the universal plot and to obtain the two moduli G_c and G_e related to the densities of cross-links and entanglements of the individual networks. The predictions of our new model are in good agreement with experimental data for uniaxially deformed polybutadiene, poly(dimethylsiloxane), and natural rubber networks, as well as with recent computer simulations.

1. Introduction

Understanding the molecular mechanisms of rubber elasticity remains one of the most important unsolved problems of polymer physics. Numerous attempts to develop a molecular description of polymer networks in the last half of a century have been only partially successful and have left the field with a dozen competing and often conflicting models. Nevertheless, several of these models introduce important physical concepts that describe many aspects of physics of polymer networks.

In this paper, we review what we believe are the most significant of these concepts and put them together into a coherent molecular picture of rubber elasticity.

First, we describe the main pieces of this theoretical puzzle—the important concepts of the existing theoretical models. In section 2, we discuss the affine and phantom models with unconstrained fluctuations of network chains. The models with constrained chain fluctuations are reviewed in section 3. We present the exact solution of the constrained-junction model and compare it with the approximate solution reported in the literature. We also review the main ideas of the tube models. In section 4, we put these pieces of the puzzle together and propose our new model of rubber elasticity—the slip-tube model. The predictions of this model are compared with those of other models and with experiments and computer simulations on uniaxial deformation in section 5. In section 6, we summarize the main ideas discussed in this paper. The notations used in this paper are collected in Appendix A. In Appendix B, we list the main results of all models discussed in this paper. In Appendix C, we derive the expression for the stress in unconstrained and constrained network models. In Appendix D, we derive the exact solution of the constrained-junction model.

2. Unconstrained Network Models

2.1. Affine Network Model. All molecular models of polymer networks are based on the microscopic picture of the entropic elasticity of chains they are made of. However, on macroscopic length scales, polymer networks deform as elastic solids. The simplest way to connect these microscopic and macroscopic pictures is to rigidly attach the ends of the chains to an *elastic nonfluctuating background*, as sketched in Figure 1. This elastic background deforms affinely and therefore this simplest model proposed by Kuhn, Wall, and Flory[1] is called the "affine network model". The affine deformation of the network chains means that the vector $\mathbf{X} \equiv \mathbf{X}_2 - \mathbf{X}_1$ between any two points $\mathbf{X}_1$ and $\mathbf{X}_2$ on this background changes proportionally to the macroscopic deformation coefficients $\{\lambda_\alpha\}$

$$X_\alpha^0 \rightarrow X_\alpha = \lambda_\alpha X_\alpha^0 \tag{1}$$

where $\alpha = x, y, z$.

The main goal of this paper is to develop a microscopic model for calculating the stress in deformed polymer networks. The stress $\sigma_{\alpha\beta}$ is proportional to the change of the network free energy density F as a result of an infinitesimal strain $\epsilon_{\alpha\beta}$

$$\sigma_{\alpha\beta} \equiv \frac{\partial F}{\partial_{\epsilon\alpha\beta}}\bigg|_{\epsilon=0} \tag{2}$$

The strain tensor ϵ describes the additional infinitesimal deformation of the elastic nonfluctuating background

$$X_\alpha \rightarrow X'_\alpha = X_\alpha + \sum_\beta \epsilon_{\alpha\beta} X_\beta \tag{3}$$

The elastic free energy of the affine network is the sum of the free energies of all its chains. The elastic free

10.1021/ma0203849 CCC: $22.00
Published on Web 07/16/2002

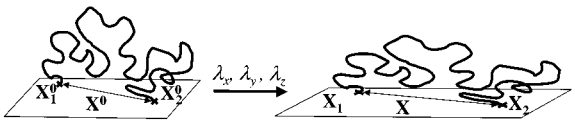

Figure 1. Affine network model. The ends of the network chains are attached to the elastic nonfluctuating background, which deforms affinely with network deformations, eq 1.

energy of one chain with ends permanently attached to the elastic background at points $\mathbf{X}_1'$ and $\mathbf{X}_2'$ is

$$F_{\mathrm{ch}}^{\mathrm{el}} = \frac{3kT}{2b^2N}(\mathbf{X}')^2 \tag{4}$$

where $\mathbf{X}' = \mathbf{X}_2' - \mathbf{X}_1'$ is the vector between the points of attachments, k is the Boltzmann constant, T is the absolute temperature, and b is the monomer size. Therefore, the elastic part of the free energy density of the affine network is the chain number density

$$\nu = c/N \tag{5}$$

times the average free energy of one chain $F_{\mathrm{ch}}^{\mathrm{el}}$ (eq 4), where c is the monomer number density and N is the degree of polymerization of the network chains.

$$F_{\mathrm{af}}^{\mathrm{el}} = \nu\frac{3kT}{2b^2N}\overline{(\mathbf{X}')^2} \tag{6}$$

A bar in eq 6 denotes the averaging over all network chains.

Substituting eq 3 into the free energy of the affine network, eq 6, and differentiating it with respect to the strain tensor $\epsilon_{\alpha\beta}$, eq 2, we obtain the expression for the elastic stress of the affine network

$$\sigma_{\alpha\beta}^{\mathrm{el}} = \nu\frac{3kT}{b^2N}\overline{X_\alpha X_\beta} \tag{7}$$

In addition to this elastic part the total stress contains an additional contribution from the pressure Π.[2]

$$\sigma_{\alpha\beta} = \sigma_{\alpha\beta}^{\mathrm{el}} - \Pi\delta_{\alpha\beta} \tag{8}$$

Consider a simple case of uniaxial deformation ($\lambda_x = \lambda_y$) with external force applied to the network in the z direction and no external forces acting in other directions. The only nonvanishing component of the total stress is σ_{zz}. From the condition of vanishing stress in x and y directions, $\sigma_{xx} = \sigma_{yy} = 0$, we find the pressure $\Pi = \sigma_{xx}^{\mathrm{el}} = \sigma_{yy}^{\mathrm{el}}$. Substituting it back into eq 8, we find the total stress in the network in z direction to be

$$\sigma_{zz} = \sigma_{zz}^{\mathrm{el}} - \sigma_{xx}^{\mathrm{el}} \tag{9}$$

The elastic stress $\sigma_{\alpha\beta}^{\mathrm{el}}$ is proportional to the end-to-end vector correlation function $\overline{X_\alpha X_\beta}$ of the deformed network, eq 7. The bar corresponds to averaging over all possible ways of attachment of network chains to the elastic nonfluctuating background at preparation conditions. In the simplest case of forming the network by end-linking chains in a melt, the end-to-end vector correlation function for undeformed network is

$$\overline{X_\alpha^0 X_\beta^0} = \frac{1}{3}b^2N\delta_{\alpha\beta} \tag{10}$$

For a network deformed according to eq 1, the correlation function becomes

$$\overline{X_\alpha X_\beta} = \frac{1}{3}b^2N\lambda_\alpha{}^2\delta_{\alpha\beta} \tag{11}$$

Combining eqs 7 and 11, we recover the celebrated expression for the elastic stress

$$\sigma_{\alpha\beta}^{\mathrm{el}} = kT\nu\delta_{\alpha\beta}\lambda_\alpha{}^2 \tag{12}$$

and using the incompressibility condition $\lambda_x = \lambda_y = \lambda^{-1/2}$, $\lambda_z = \lambda$, we find the total stress

$$\sigma_{zz} = kT\nu(\lambda^2 - \lambda^{-1}) \tag{13}$$

of the affine network model. It is important to realize that in the affine network model the ends of network chains are directly attached to the elastic nonfluctuating background and therefore do not fluctuate. In more realistic network models, these fluctuations are taken into account and make an additional contribution to the stress.

2.2. Phantom Network Model. One of the earliest models that took into account the fluctuations of chain ends was the "phantom network model" of James and Guth.[3] Instead of connecting the ends of network chains directly to the elastic background, they were attached to each other at cross-links (or junctions). Macroscopic deformation is transmitted to the bulk of the network through the chains attached to its surface. In this model, the cross-links in the bulk of the network fluctuate around their average positions (see Figure 2a). The magnitude of these fluctuations determines how strongly the macroscopic deformation of the network is coupled to the deformation of individual chains. The mean square fluctuation of the end-to-end vector $\mathbf{R}$ around its average value $\langle\mathbf{R}\rangle$ depends on the functionality ϕ of junctions[4,5]

$$\langle(\Delta\mathbf{R})^2\rangle \equiv \langle(\mathbf{R} - \langle\mathbf{R}\rangle)^2\rangle = \frac{2}{\phi}b^2N \tag{14}$$

As expected, the fluctuations of chain ends decrease with increasing functionality ϕ.

The single-chain description of the phantom network which maps it onto the affine network model was proposed recently in ref 6. In this description individual chains are connected to the elastic background through the *effective chains*. In the undeformed state ($\lambda_\alpha = 1$), the points of attachment of these effective chains to the elastic background are randomly distributed because of the randomness of the cross-linking process. Since effective chains are attached to the nonfluctuating background, the points of attachment deform affinely with the network deformations, see eq 1. A network chain with its two effective chains together define a *combined chain* (Figure 2b).

The effective chains control the fluctuations of the ends of the network chains and represent the way elasticity is transmitted from macroscopic scales down to the individual chains. The mean square fluctuations of the end-to-end vector $\mathbf{R}$ of a network chain connected to the elastic background by two identical effective chains with the degree of polymerization n each are equal to[6]

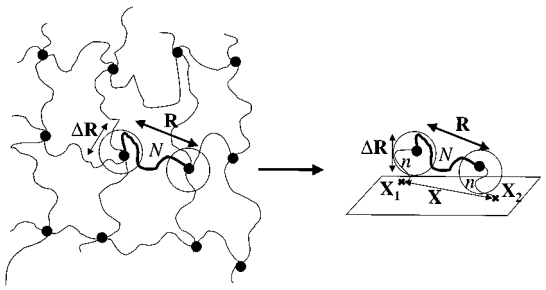

Figure 2. Phantom network model is equivalent to the affine network model of combined chains. Each combined chain consists of one network chain and two effective chains.

$$\langle(\Delta\mathbf{R})^2\rangle = \frac{b^2}{1/N + 1/(2n)} \tag{15}$$

From the comparison of the two estimates of the mean square cross-link fluctuations, eqs 14 and 15, we find the dependence of the number of monomers n of effective chains on the network functionality ϕ

$$n = \frac{N}{\phi - 2} \tag{16}$$

The phantom network model is therefore equivalent to the affine network model of combined chains. Each of these combined chains consists of one network chain and two effective chains (see Figure 2).

As shown in Appendix C, the expression (eq 7) for the elastic stress of the affine model can be generalized to that for the phantom network model and becomes

$$\sigma^{\mathrm{el}}_{\alpha\beta} = \nu\frac{3kT}{b^2 N}\overline{\langle R_\alpha R_\beta\rangle} - \mu kT\delta_{\alpha\beta} \tag{17}$$

where

$$\mu = 2\nu/\phi \tag{18}$$

is the concentration of cross-links. The main difference between the equations for stress in the two models (eqs 7 and 17) is that the correlation function of the nonfluctuating end-to-end vector of the affine model $\overline{X_\alpha X_\beta}$ is replaced by the one of fluctuating end-to-end vector of the phantom network model $\overline{\langle R_\alpha R_\beta\rangle}$. Angular brackets represent averaging over thermal fluctuations.

The correlation function of the end-to-end vector is the sum of two correlation functions

$$\overline{\langle R_\alpha R_\beta\rangle} = \overline{\langle R_\alpha\rangle\langle R_\beta\rangle} + \overline{\langle \Delta R_\alpha \Delta R_\beta\rangle} \tag{19}$$

In the combined chain model, the average value of the end-to-end vector $\langle R_\alpha\rangle$ is proportional to the distance between the points of attachments of this combined chain to the elastic background.

$$\langle\mathbf{R}\rangle = \frac{N}{N + 2n}\mathbf{X} \tag{20}$$

The coefficient of proportionality is the ratio of the number of monomers N of the network chain to the total number of monomers $N + 2n$ of the combined chain. The second correlation function in eq 19 can be easily obtained from eq 15 by realizing that fluctuations of different components of a Gaussian chain are not correlated

$$\overline{\langle \Delta R_\alpha \Delta R_\beta\rangle} = \frac{\delta_{\alpha\beta}}{3}\langle(\Delta\mathbf{R})^2\rangle = \frac{\delta_{\alpha\beta}}{3}\frac{b^2}{1/N + 1/(2n)} \tag{21}$$

Combining eqs 17−21, we find the elastic stress of a deformed phantom network

$$\sigma^{\mathrm{el}}_{\alpha\beta} = \nu\frac{3kT}{b^2}\frac{N\overline{X_\alpha X_\beta}}{(N + 2n)^2} + kT\delta_{\alpha\beta}\left(\frac{2n\nu}{N + 2n} - \mu\right) \tag{22}$$

The concentration of cross-links is $\mu = 2\nu/\phi$ (eq 18) and the second term of eq 22 is equal to zero for phantom networks. This is due to a simple relation (eq 16) between the number of monomers n in effective chains and network functionality ϕ. This term becomes nonzero in more complicated models (e.g., see eq 30 below).

The correlation function $\overline{X_\alpha X_\beta}$ of the phantom network model can be obtained from the correlation function of the affine model by substituting the number of monomers $N + 2n$ of the combined chain for the degree of polymerization N in eq 11. The resulting expression for the stress of the deformed network is

$$\sigma^{\mathrm{el}}_{\alpha\beta} = kT\nu\frac{N}{N + 2n}\delta_{\alpha\beta}\lambda_\alpha{}^2 = kT\left(1 - \frac{2}{\phi}\right)\nu\delta_{\alpha\beta}\lambda_\alpha{}^2 \tag{23}$$

Note that the functional dependence of the elastic stress on the deformation coefficients $\{\lambda_\alpha\}$ is the same for both phantom and affine network models, eqs 23 and 12; the only difference is in the prefactors. The coefficient $(1 - 2/\phi)\nu = \nu - \mu$ in eq 23 is the difference between the number densities of chains and cross-links. In a more general case of an imperfect network (with dangling chains and loops), this coefficient becomes the difference between the number densities of elastically effective chains ν and cross-links μ.[7,8]

$$\sigma^{\mathrm{el}}_{\alpha\beta} = kT(\nu - \mu)\delta_{\alpha\beta}\lambda_\alpha{}^2 \tag{24}$$

Elastically effective are the chains which deform and store elastic energy upon network deformations and elastically effective cross-links are those that connect at least two elastically effective chains.

Note that the variation of the diagonal components of the strain tensor $\epsilon_{\alpha\alpha}$ can be expressed through the variation of the deformation coefficient, $d\epsilon_{\alpha\alpha} = d\lambda_\alpha/\lambda_\alpha$, and eq 2 for elastic stress takes the form

$$\sigma^{\mathrm{el}}_{\alpha\alpha} = \lambda_\alpha\frac{\partial F^{\mathrm{el}}}{\partial\lambda_\alpha} \tag{25}$$

Substituting eq 23 into eq 25 and integrating it with respect to λ_α, we reproduce the famous expression for the elastic free energy of the phantom network model

$$F^{\mathrm{el}}_{\mathrm{ph}}(\lambda) = \frac{kTc}{2N}\left(1 - \frac{2}{\phi}\right)\sum_\alpha \lambda_\alpha{}^2 \tag{26}$$

Both affine and phantom network models give a very good qualitative picture of rubber elasticity. But quantitative comparison of their predictions with experiments shows that some essential physics is not included in these models. A long time ago, it was realized that topological interactions between network chains make an important contribution to rubber elasticity. Unfortunately, there is no rigorous description of topological

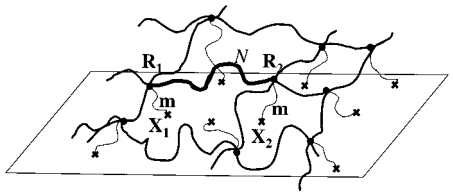

Figure 3. Constrained-junction model. Cross-links of network chains are connected to the elastic nonfluctuating background by virtual chains (thin lines).

entanglements, and different models of polymer networks take them into account using different assumptions.

3. Constrained Network Models

3.1. Exact Solution of the Constrained-Junction Model. One of the standard models that attempts to account for the topological intermolecular interactions is the "constrained-junction model".[9−14] Entanglements of a network chain with its neighbors restrict its fluctuations. In the constrained-junction network, this effect is modeled by an additional harmonic potential acting on the cross-links of the phantom network. This potential reduces the fluctuations of network chains by restricting the fluctuations of cross-links. The confining potential can be represented by confining *virtual chains* connecting cross-links to the elastic background; see Figure 3. The points of attachments of these virtual chains to the elastic background are chosen in such a way as to keep the Gaussian statistics of network chains in the preparation condition. The space available for chain fluctuations changes upon network deformations, since chains move further apart or closer together. To take this effect into account, the potential acting on the cross-links is assumed to change with the deforming network.

Many large-scale physical properties of polymers are not affected by the microscopic representation of the monomers they are made of. For example, chain elasticity of the rotational isomeric state, freely joined, or lattice models of polymers are identical for chains with the same Kuhn length and the same number of Kuhn segments. The only difference between models is expected in the region of almost fully extended chains (with $R \approx bN$). To define confining virtual chains for anisotropically deformed networks we consider the *lattice model* of polymers. In this model each monomer can be directed only along one of three major axis, x, y, or z, of network deformation. Monomers in this model are located at the lattice sites and numbered (0, 1, ..., s, ..., N) from one end of the chain. The index s corresponds to the number of bonds in the chain between its beginning monomer 0 and sth monomer. We would like to be more specific and count bonds directed along each of the axes separately. In this case the monomer s would be characterized by three indexes, s_x, s_y and s_z—numbers of bonds directed along the x, y, and z axes between the beginning of the chain (number 0) and the monomer $s = s_x + s_y + s_z$. This definition allows one to "split" a 3-dimensional chain into three independent 1-dimensional ones. The α component of the coordinate $R_\alpha(s_\alpha)$ of the monomer with indexes (s_x, s_y, s_z) depends only on index s_α. The length of the section of the chain between monomers 0 and $s = s_x + s_y + s_z$, is proportional to the sum of all three indexes, $b(s_x + s_y + s_z)$. Each of these indexes s_α varies in the interval $0 < s_\alpha < N_\alpha$, where N_α is the number of chain monomers along the axis α, and the total number of monomers of the chain is $N = N_x + N_y + N_z$. For the unconstrained chain all these numbers are (on average) equal, $N_x^0 = N_y^0 = N_z^0 = N/3$, and they can be different only in the presence of orientational ordering field of nematic, electric, or topological—in our case—nature.

The new important physical concept introduced in the constrained-junction model is that fluctuations of virtual chains representing this effective confining potential deform affinely with the network.[9−14] The amplitude of fluctuations of Gaussian virtual chains is proportional to the square root of the number of "virtual" monomers m. The assumption of the *affine deformation of fluctuations* implies that the number of monomers along the axis α of virtual chains changes with network deformation as

$$m_\alpha = \frac{1}{3} m^0 \lambda_\alpha^{\,2} \tag{27}$$

Note that the confining potential is isotropic in the undeformed state but becomes anisotropic upon anisotropic deformation of the network. This anisotropic potential is represented by the different number of virtual monomers m_α confining cross-link fluctuations in different directions.

The elastic stress of the constrained-junction model has exactly the same form as that in the phantom model, eq 17. This result can be derived by differentiating the elastic free energy of both models with respect to the infinitesimal deformation tensor, eq 2 (see Appendix C). The same result can be obtained from the definition of the stress tensor $\sigma_{\alpha\beta}$ as the αth component of the force acting per unit area perpendicular to the βth axis.[15] It is important to realize that *the two derivations lead to the same expression for the elastic stress* $\sigma_{\alpha\beta}^{el}$ *of the constrained-junction model if and only if the number of monomers in confining virtual chains changes with deformation of the network as prescribed in eq 27*. This verifies the self-consistency of the constrained-junction model.

Note that confining virtual chains do not directly contribute to the stress in eq 17, which is only supported by network chains. Confining virtual chains only change the conformations of real network chains and thus, the distribution function over which the averaging is taken in eq 17.

An approximate solution of the constrained-junction model (see Appendix B) was described in a number of papers[10−12] and was later used in several generalizations of this model.[16,17] Below, we present the exact solution of this model.

The constrained-junction model can be reduced to the combined chain model consisting of the network chain and two effective chains. Each of these effective chains contains n_α monomers directed along the α axis. The total number of monomers in each of these effective chains is $n_x + n_y + n_z$. The exact expression for the number of monomers of the effective chain directed along the α axis is derived in Appendix D

$$\frac{1}{n_\alpha} = \frac{1}{2}\left\{\frac{1}{n_\alpha^{||}} + \sqrt{\frac{1}{(n_\alpha^{||})^2} + \frac{4}{N_\alpha^0 m_\alpha}}\right\} \tag{28}$$

where $n_\alpha^{||}$ is defined below in eq 29. A simple estimate of the number of monomers n_α of each of these effective

chains can be obtained from the picture of the parallel connection of the phantom effective chain with $N_\alpha^0/(\phi - 2)$ monomers (eq 16) and the confining virtual chain with m_α monomers (eq 27). These two parallel virtual chains can be replaced by a single effective one with the degree of polymerization $n_\alpha^{||}$:

$$\frac{1}{n_\alpha^{||}} \equiv \frac{\phi - 2}{N_\alpha^0} + \frac{1}{m_\alpha}, \quad N_\alpha^0 = \frac{N}{3} \tag{29}$$

Approximating n_α by $n_\alpha^{||}$ ignores the confining virtual chains attached to other cross-links beside the two at the ends of the chosen network chain. Below, we will use the exact expression for n_α (eq 28).

The stress of the constrained-junction model in the combined chain representation is of the identical form to that of the phantom model, eq 22. The only difference is the replacement of the numbers of monomers of the network chains N and of the effective chains n of the phantom network model by the corresponding numbers N_α^0 and n_α of the constrained-junction model.

$$\sigma_{\alpha\beta}^{el} = \nu\frac{3kT}{b^2}\frac{N_\alpha^0\overline{X_\alpha X_\beta}}{(N_\alpha^0 + 2n_\alpha)(N_\beta^0 + 2n_\beta)} + kT\delta_{\alpha\beta}\left(\frac{2n_\alpha\nu}{N_\alpha^0 + 2n_\alpha} - \mu\right) \tag{30}$$

The correlation function $\overline{X_\alpha X_\beta}$ of the components of the vector between points of attachment of the combined chain to the elastic background is calculated in Appendix D. In this appendix, it is shown that substitution of eq D10 into eq 30 leads to the exact expression for the elastic stress of the constrained-junction model (eq D19):

$$\sigma_{\alpha\beta}^{el} = kT\delta_{\alpha\beta}\nu\left[1 - \frac{2}{\phi} + (\lambda_\alpha{}^2 - 1)\left(\frac{1 - z_\alpha}{1 + z_\alpha}\right)^2\frac{1 + z_\alpha{}^2(\phi - 1)}{1 - z_\alpha{}^2(\phi - 1)}\right] \tag{31}$$

where

$$z_\alpha = \frac{n_\alpha}{N_\alpha^0 + n_\alpha} \tag{32}$$

The exact expression for the free energy of this model is given in eq D20 of Appendix D.

To compare the exact expression for the stress of the constrained-junction model, eq 31, with the approximate one,[10−12] we introduce the Mooney ratio of the total stress $\sigma_{zz} = \sigma_{zz}^{el} - \sigma_{xx}^{el}$ to the functional dependence $\lambda^2 - \lambda^{-1}$ predicted by models with unconstrained fluctuations of network chains (e.g., affine and phantom network models):[18]

$$f^*(\lambda_z{}^{-1}) = \frac{\sigma_{zz}^{el} - \sigma_{xx}^{el}}{\lambda^2 - \lambda^{-1}} \tag{33}$$

In Figure 4, we plot the Mooney ratio, eq 33, for the exact (eq 31) and for the approximate (see Appendix B) solutions of the constrained-junction model with functionality $\phi = 4$. The exact solution is represented by solid curves while the approximate one is shown by dashed curves. The numbers next to each pair of curves give the value of the parameter N/m^0, which characterizes the relative strength of the confining potential. Large values of this parameter correspond to the network with junction points strongly coupled to the elastic background as in the affine network model. In this case the Mooney ratio approaches νkT. In the opposite case of very weak confining potential the junction points fluctuate as in the phantom network model and the Mooney ratio approaches $(1 - 2/\phi)\nu kT$. Therefore, the affine and the phantom network models are the two limiting cases of the constrained-junction model. Although the approximate solution captures all the main qualitative features of the exact solution, it deviates from it by ~20%. Note also that the peak at intermediate values of the parameter N/m^0 is more pronounced in the exact solution.

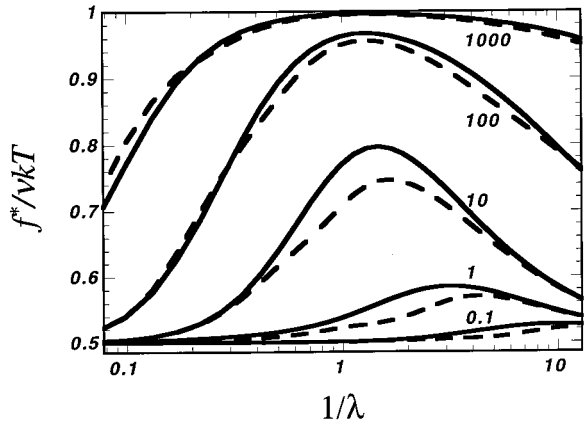

Figure 4. Comparison of exact (solid lines) and approximate (dashed lines) solutions of the constrained-junction model with functionality $\phi = 4$. The numbers correspond to the relative strength N/m^0 of the confining potential.

The constrained-junction model represents the topological interactions between network chains by imposing additional restrictions on the fluctuations of junctions. In the limit of a very strong topological confining potential ($N/m^0 \to \infty$), the fluctuations of junctions are completely suppressed. However, even in this case, other monomers of the chain are not constrained, and therefore, their fluctuations are almost unchanged. This is not a realistic representation of real topological interactions in polymer networks. Another attempt to further restrict the fluctuations of the chain was made in the "constrained-chain model".[16,17] In this model, in addition to topological potentials acting on cross-links, one adds topological potential acting on the centers of mass of the network chains. Though this additional potential further restricts fluctuations of monomers, it is still not sufficient to represent real topological interactions between chains.

3.2. Diffused-Constraint Model. An attempt to make the confining potential affect fluctuations of all points along the network chain was made in the "diffused-constraint model".[19] In this model, topological constraint (confining virtual chain) is applied to a single monomer of the chain, and the free energy of such a constrained chain is averaged over all possible locations of this monomer along the chain. This procedure was described as "diffusing of constraints so as to include fluctuations of all such points along the chain" since the averaging was interpreted as the sum of independent contributions of many confining virtual chains distrib-

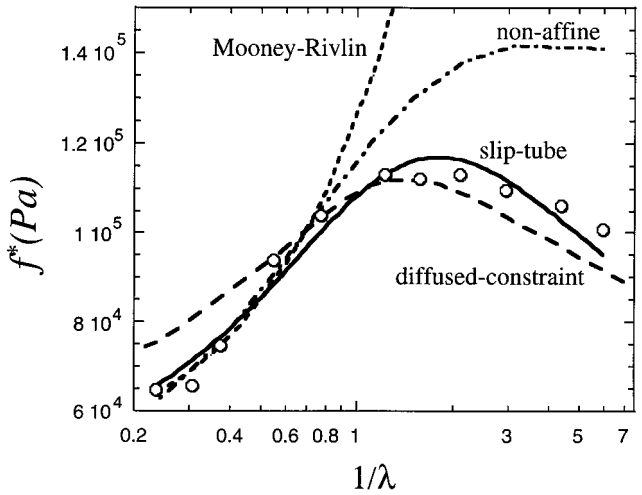

Figure 5. Fit of the data by Pak and Flory[20] on cross-linked poly(dimethylsiloxane) (open circles) by the diffused-constrained model (dashed line), Mooney−Rivlin expression (dotted line), nonaffine tube model (dash−dotted line), and the slip-tube model (solid line).

uted along the network chain. Unfortunately, this interpretation is incorrect because it ignores the connectivity of the chain and therefore does not take into account the correlations between fluctuations of virtual chains. In fact, the diffused-constraint model describes a network, each chain of which is connected by only one confining virtual chain to the elastic background. The location along the network chain of its single junction with the virtual chain varies from one network chain to another one. This single connection with the virtual chain is not enough to represent topological entanglements, and the diffused-constraint model is analogous to the constrained-chain and constrained-junction models.

The approximate solution of the diffused-constraint model[19] is given in Appendix B. The Mooney ratio (eq 33) plot of this approximate solution is compared with the experimental data of Pak and Flory[20] on uniaxially deformed cross-linked poly(dimethylsiloxane) and with the predictions of other models in Figure 5. The best fit of the experimental data (represented by open circles) by the diffused-constraint model (with fitting parameters $N/m^0 = 17$ and $kT\nu = 1.34 \times 10^5$ Pa) is the dashed line. The best fit of the elongation part of the data ($\lambda > 1$) by the Mooney−Rivlin expression $f^* = 2C_1 + 2C_2/\lambda$ (with fitting parameters $C_1 = 2.2 \times 10^4$ Pa and $C_2 = 4.0 \times 10^4$ Pa) is the dotted line. The fit of the elongation part of the data by the nonaffine tube model (see eq 44) below) with fitting parameters $G_c = 3.7 \times 10^4$ Pa and $G_e = 7.9 \times 10^4$ Pa is the dash−dotted line. The solid line is the fit of all experimental data in Figure 5 by our new slip-tube model (see eq 60 below) with fitting parameters $G_c = 4.5 \times 10^4$ Pa and $G_e = 6.3 \times 10^4$ Pa. The fit of the experimental data by the diffused-constraint model is better than that by the Mooney−Rivlin expression or by the nonaffine tube model,[21] but not as good as that by the slip-tube model. The narrowest possible peak predicted by the expression for the diffused-constraint model (see Appendix B) is at a value of the parameter $N/m^0 \cong 17$, but the predicted peak is still too broad in comparison with experimental data (and with the prediction of the slip-tube model). A similar conclusion was reached from the comparison of these models with six additional sets of experimental data on uniaxial deformation because of the universal shape of the data demonstrated in section 5 below.

The main problem with the diffused constrained model is the same as with the constrained chain and the constrained-junction models. All of these models impose only limited constraints on chain fluctuations. Constrained-junction model restricts fluctuations of junction points. The constraint chain model restricts fluctuations of junctions and of the center of mass of network chains. The diffused constraint model restricts fluctuations of a single randomly chosen monomer for each network strand. Thus, all these models can only represent the crossover between the phantom and affine limits, as discussed in section 3.1 and shown in Figure 4 for the constrained-junction model. The affine limit corresponds to a very strong constraining case, and the phantom limit corresponds to a weak constraining potential. As is clear from Figure 4, the Mooney function (eq 33) of these models can only change by a factor of 2 (for $\phi = 4$) because these models are in the crossover between the affine and phantom limits. This is the reason the diffused constraint model changes less than the experimental data of Figure 5. We conclude that this model can only provide a reasonable description of weakly entangled polymer networks.

3.3. Edwards' Tube Model. The realistic model of the topological constrains should take into account the fact that they act along the whole chain and restrict the fluctuations of all monomers of the chain. The most successful way of representing these topological entanglements is the "Edwards tube model".[22] In this model the topological potential is applied to every monomer of the chain, effectively restricting its fluctuations to a *confining tube*. In the Edwards tube model, this potential does not change upon network deformations and can be represented by confining virtual chains connecting every network monomer to the elastic background.[6] The degree of polymerization m of these confining virtual chains is assumed to be independent of the network deformation. The same effective confining potential can be represented by shorter confining virtual chains of $m(p)$ monomers connecting every pth monomer of the network chain to the elastic background.[6] These confining virtual chains restrict the fluctuations of network monomers to a tube with the diameter

$$a \simeq bN_e^{1/2} \simeq b[pm(p)]^{1/4} \tag{34}$$

where N_e is the degree of polymerization between entanglements of the network chain. From eq 34, it follows that the number of monomers of the confining virtual chains is $m(p) \simeq N_e^2/p$. In order for the fluctuations of network monomers to be unaffected by this choice of confining virtual chains, the inequality $p \leq N_e$ has to be satisfied. For a qualitative understanding of this tube model, it is convenient to choose confining virtual chains with $m(p) \simeq N_e$ monomers and with points of attachment separated by $p \simeq N_e$ monomers along the network chain.

Consider the case of a highly entangled network, $N/N_e \gg 1$, with many entanglements per network chain. The behavior of the entangled strand in the Edwards tube model can be represented by the combined chain, as shown in Figure 6. The combined chain consists of an entangled strand of p real monomers connected to the elastic nonfluctuating background through two effective

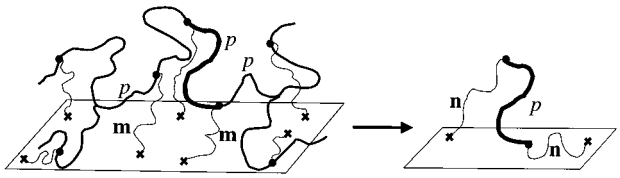

Figure 6. Confining tube model. Every *p*th monomer of the network chains (intermediate and thick lines) is connected to the elastic nonfluctuating background by virtual chains containing *m* monomers each. In the combined chain representation, the strand of *p* real monomers is connected to the elastic background by two effective chains containing *n* virtual monomers.

chains containing $n \approx N_e$ virtual monomers. The number of virtual monomers in the Edwards tube model does not change upon deformation (n is independent of λ). The stress in this model can be found by the analogy with that of the phantom chain model (eq 23)

$$\sigma_{\alpha\beta}^{el} = kT\frac{c}{p}\frac{p}{p+2n}\delta_{\alpha\beta}\lambda_\alpha^{\ 2} = kT\frac{c}{N_e}\delta_{\alpha\beta}\lambda_\alpha^{\ 2} \qquad (35)$$

where the number of monomers between entanglements, N_e, is equal to the degree of polymerization of the combined chain, $N_e = p + 2n$.

Although the Edwards tube model captures the physics of the continuous distribution of constraints along the chain, the assumption of deformation-independent confining potential contradicts both theoretical and experimental observations. The confining virtual chains were introduced only to restrict the fluctuations of network chains and they cannot carry any real stress. From the microscopic definition of stress, it follows that eq 35 gives only part of the total stress, carried by real chains. In the Edwards tube model, the total stress has an additional contribution from virtual chains, which is in disagreement with the microscopic picture of stress. The Edwards tube model predicts strain-independent Mooney ratio f^* (λ^{-1}), eq 33, which is not in agreement with experiments.

3.4 Nonaffine Tube Model. An accurate estimate of the free energy of a chain confined to the deformation dependent tube was made recently in ref 6 within the framework of the "nonaffine tube model". This model is similar to the classical Edwards tube model. Every *p*th monomer of the chain is attached to the elastic background by a confining virtual chain; see Figure 6. There are two major differences between the two tube models:

1. In the Edwards tube model, the points of attachments of confining virtual chains to the elastic background are placed along the well-defined contour of the tube. In the nonaffine tube model, they are randomly distributed in space in order to guarantee the Gaussian statistics of the network chain at the preparation conditions.

2. In the Edwards tube model, the amplitude of fluctuations of confining virtual chains is independent of network deformation. In the nonaffine tube model, it changes proportionally to the network deformation. This implies that in the nonaffine tube model the number of monomers of confining virtual chains along the axis α is $m_p = m_p^0\lambda_\alpha^2$; see eq 27. In Appendix C, we prove that this is the only possible assumption consistent with the microscopic definition of the stress tensor.

Both of the above assumptions about the confining potential are the same as in the constrained-junction model; see section 3.1. The difference is that in the nonaffine tube model this potential acts not only on cross-links but also on every monomer of the network chains. The stress of the nonaffine tube model in the highly entangled limit $N \gg N_e$ is identical to the stress of the constrained-junction network model with the functionality $\phi = 2$. The number of monomers of the effective chains n_α along the axis α can be obtained from eq 28 by substituting the degree of polymerization of the constrained-junction network chains N and confining virtual chains m_0 by the number of monomers between neighboring strands of network chains p and that of confining virtual chains m_p of the nonaffine tube model

$$n_\alpha = \frac{1}{6}(\sqrt{p^2 + N_e^{\ 2}\lambda_\alpha^{\ 2}} - p) \qquad (36)$$

where $N_e \equiv 2\sqrt{pm_p}$. The parameter z_α of the nonaffine tube model can be obtained from eq 32 by a similar substitution.

$$z_\alpha = \frac{\sqrt{p^2 + N_e^{\ 2}\lambda_\alpha^{\ 2}} - p}{\sqrt{p^2 + N_e^{\ 2}\lambda_\alpha^{\ 2}} + p} \qquad (37)$$

The stress of the nonaffine tube model can be obtained from the stress of the constrained-junction network model with the functionality $\phi = 2$ by substituting parameter z_α from eq 37 into eq 31.

$$\sigma_{\alpha\beta}^{el} = kTc\delta_{\alpha\beta}(\lambda_\alpha^{\ 2} - 1)\frac{p^2 + N_e^{\ 2}\lambda_\alpha^{\ 2}/2}{(p^2 + N_e^{\ 2}\lambda_\alpha^{\ 2})^{3/2}} \qquad (38)$$

The stress (eq 38) can be simplified in the limit $p \ll N_e\lambda_\alpha$ when confining virtual chains are densely attached to the network one.

$$\sigma_{\alpha\beta}^{el} = kT\delta_{\alpha\beta}\frac{c}{2N_e}\left(\lambda_\alpha - \frac{1}{\lambda_\alpha}\right) \qquad (39)$$

In this limit, the number of monomers along the axis α of the effective chain (eq 36) becomes

$$n_\alpha = \frac{1}{6}N_e\lambda_\alpha = N_\alpha^{aff} \qquad (40)$$

This effective chain has the same number of monomers as the affine strand of the network chain N_α^{aff}. The size of the affine strand defines the affine length scale[6] along the axis α

$$R_\alpha^{aff} = \lambda_\alpha b\sqrt{N_\alpha^{aff}} \simeq bN_e^{\ 1/2}\lambda_\alpha^{3/2} \qquad (41)$$

The network deforms affinely as an elastic solid on length scales longer then R_α^{aff}. On length scales shorter than R_α^{aff}, the confining potential has very little effect on conformations of individual network chains. The amplitude of fluctuations of the affine strand defines the tube diameter

$$a_\alpha = b\sqrt{N_\alpha^{aff}} \simeq bN_e^{\ 1/2}\lambda_\alpha^{\ 1/2} \qquad (42)$$

One of the main results of the nonaffine tube model is that the tube diameter changes with network deformation and is anisotropic for the anisotropically deformed networks. A similar dependence of the tube diameter

on the network deformation was obtained in refs 23 and 24. The fluctuations of the affine strand are confined by entanglements and therefore the tube diameter a_α along the axis α is equal to the distance between entanglements—the size of the deformed strand of N_e monomers, $a_\alpha = (N_e/N^{aff})R_\alpha^{aff}$.

Integrating eqs 25 and 39, we find the elastic free energy of the nonaffine tube model[6]

$$F_{naf}^{el}(\lambda) = F_{ph}^{el}(\lambda) + \frac{ckT}{2N_e}\sum_\alpha \left(\lambda_\alpha + \frac{1}{\lambda_\alpha}\right) \qquad (43)$$

The first term in eq 43 is introduced in order to describe the contribution due to cross-links (free energy of the phantom network model, eq 26). The second term in eq 43 is the contribution of entanglements in the nonaffine tube model. Expression 39 shows that the stress−strain dependence becomes nonlinear.[18] The prediction for the Mooney ratio (eq 33) of the nonaffine tube model

$$f^*(\lambda^{-1}) = G_c + \frac{G_e}{\lambda - \lambda^{1/2}+1} \qquad (44)$$

is in much better agreement with experiments on uniaxial compression than the Mooney−Rivlin expression (see Figure 5). Nevertheless, the maximum of the normalized stress on the Mooney plot predicted by the nonaffine tube model is not as pronounced as in experiments.[21]

In the nonaffine tube model, the virtual chains are permanently attached to the network chains. This eliminates the possibility of slippage of the network chain and the redistribution of its monomers along the contour of the tube. This slippage mechanism leads to the main modes of stress relaxation in polymer melts—reptation and tube length fluctuations. It is natural to expect that the redistribution of chain length along the tube contour will also be important in anisotropically deformed highly entangled networks. Below, we modify the nonaffine tube model to include these degrees of freedom and demonstrate that the new model is in better agreement with experimentally measured stress of uniaxially deformed networks.

4. Slip-Tube Model

The distribution of chain length along the contour of the tube has been studied within the framework of the slip-link models.[8,25] The major difference between slip-link and tube models is the assumptions made in these models about the nature of topological entanglements. In tube models the confining potential acting on a given network strand is assumed to be formed collectively by many neighboring strands. This justifies the use of the mean field description of topological entanglements within the framework of tube models. In slip-link models each entanglement is postulated to be formed by a pair of chains.

The main idea of the slip-link models is that entanglements, which are permanently trapped by the cross-linking process, act as slip-links connecting neighboring chains. These slip-links are allowed to slide along the contour of the two chains they are linking together. In the standard approach, the slip-links are allowed to pass through each other but each of them can slide along the chain only up to a certain fixed distance. This distance is treated as an adjustable parameter of the model. If it is small compared to the average distance between neighboring slip-links, the slip-links act as chemical cross-links and the model is reduced to the phantom network one. In the opposite limit of large sliding distance, the slip-links pass through each other and the topological constrains are locally released. For the maximum allowed sliding distance along the network chain (equal to the chain length) the slip-link model is reduced to the phantom network model with pairwise associating strands.

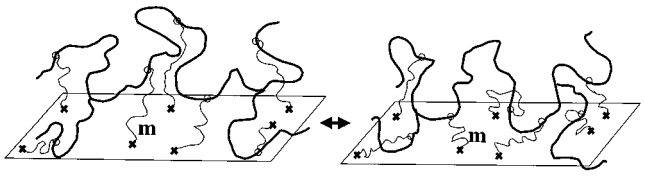

Figure 7. Slip-tube model. Confining potential acting on network chains is represented by virtual chains attached to the elastic nonfluctuating background at one end and ending with slip-links at the other. These slip-links can slide along the network chain, but cannot pass through each other.

Below, we combine the ideas of the confining tube and slip-link models to a new "slip-tube model" of polymer networks. In the original model of the tube,[22] there was no redistribution of the chain length between different sections of the tube. The idea of slippage of the chain along the contour of the tube was proposed by de Gennes in the reptation model of polymer melts.[26] The first analysis of the redistribution of the stored length along the contour of the tube was made by Doi in the framework of the "tube length fluctuation model".[27] Below, we introduce the degrees of freedom corresponding to the *slippage of the chain along the tube contour* to the nonaffine tube model[6] described in the previous section.

To allow the network chain to slide along the contour of the tube, we replace permanent attachment junctions between virtual and network chains by effective slip-links. All virtual chains defining confining potential are thus attached to the elastic background at one end and have virtual slip-links at the other end; see Figure 7. The network chain must pass through these slip-links at the fluctuating end of virtual chains in a fixed order. These slip-links can freely slide along the contour of the chain but they are not allowed to pass through each other. Therefore, the amplitude of slip-link fluctuations along the contour of the chain in the slip-tube model depends on the density of these slip-links. This density is defined as the reciprocal average number of monomers between neighboring slip-links, L/N, where L is the total number of slip-links per network chain of N monomers. For a very high density, $L = N$, the slip-links are located at every monomer, and since they are not allowed to pass through each other, the slippage is completely suppressed. In this limit, the slip-tube model reduces to the already discussed nonaffine tube model, section 3.4. In the opposite physical limit, $N/L = N_e$, the amplitude of fluctuations of a typical monomer along the contour of the tube is on the order of $b\sqrt{N}$. In this limit, there is no confining potential along the contour of the tube and therefore the amplitude of fluctuations is the Gaussian size of the network strand. Note that the same confining slip-tube, but with free boundary conditions at the ends of the chain, becomes the classical reptation model with tube length fluctuations.[15,27]

If the slippage along the tube is forbidden, the elastic free energy of the nonaffine tube model is split into three

independent contributions from the three major directions of deformation; see eq 43.

$$F^{el}_{naf}(\lambda) = F^{el}_{ph}(\lambda) + kT\frac{\nu L}{2}\sum_{\alpha}\left(\lambda_\alpha + \frac{1}{\lambda_\alpha}\right) \qquad (45)$$

This is due to the implicit assumption that the number of monomers contributing to the network elasticity is fixed to be the same in all three directions, $N^0_x = N^0_y = N^0_z = N/3$ and does not change upon deformation. In anisotropically deformed networks the sections of the tube oriented in different directions deform anisotropically. For example, for uniaxial extension, the sections of the tube oriented in the direction of network elongation are stretched, while the sections oriented in perpendicular directions are compressed. If the slippage along the tube is allowed, the extra chain length stored in the compression direction will be pulled out into the section of the tube in the elongation direction, releasing part of the stress. For a general network deformation, the chain slippage redistributes the total number of monomers N between different directions. In an anisotropically deformed network the three numbers N_x, N_y, and N_z will, in general, be different, but their sum is conserved, $N_x + N_y + N_z = N$.

We would like to stress again that all features of network elasticity originate from the entropic elasticity of chains forming the network. In the framework of the lattice model, the elastic free energy of a chain of N^0_α monomers along the axis $\alpha = x, y, z$ is

$$F^{el}_{ch} = kT\sum_{\alpha}\int_0^{N^0_\alpha}\frac{ds_\alpha}{2b^2}\left(\frac{dR_\alpha(s_\alpha)}{ds_\alpha}\right)^2 \qquad (46)$$

where $R_\alpha(s_\alpha)$ is the αth coordinate of the monomer with index $\mathbf{s} = (s_x, s_y, s_z)$. In the anisotropically deformed network the total number N_α of chain monomers in a given direction α is changed due to the slippage, $N^0_\alpha \rightarrow N_\alpha \equiv g_\alpha N^0_\alpha$. We can reassemble these monomers into groups of g_α network monomers each. We will now have the same number N^0_α of new "renormalized" monomers, each containing g_α original network monomers. The index s'_α of a renormalized monomer can be obtained from the one (s_α) for the original monomers by

$$s_\alpha \rightarrow s'_\alpha = s_\alpha/g_a, \quad g_x + g_y + g_z = 3 \qquad (47)$$

In order for the elastic free energy, eq 46, to be invariant upon such regrouping of monomers, the size of new renormalized monomers in the αth direction should be

$$b \rightarrow b'_\alpha = b g_\alpha^{1/2}, \quad g_\alpha \equiv N_\alpha/N^0_\alpha \qquad (48)$$

This change of the elementary length b of the network elasticity by the factor of $g_\alpha^{1/2}$ implies the rescaling of deformation coefficients

$$\lambda_\alpha \rightarrow \lambda'_\alpha = \frac{b}{b'_\alpha}\lambda_\alpha = \frac{\lambda_\alpha}{g_\alpha^{1/2}} \qquad (49)$$

Such renormalization of deformation coefficients has a simple physical meaning: chains with a larger number of monomers $N_\alpha = N^0_\alpha g_\alpha > N_\alpha$ placed in the same volume will be less stretched ($\lambda'_\alpha < \lambda_\alpha$) than the initial chain of N^0_α monomers.

Now we can use all the results of the nonaffine network model of section 3.4 with the above rescaling, eqs 47−49. Substituting eq 49 into the stress of the nonaffine tube model, eq 39, we find the following expression for the elastic stress of the slip-tube model

$$\sigma^{el}_{\alpha\beta} = kT\delta_{\alpha\beta}\frac{\nu L}{2}\left(\frac{\lambda_\alpha}{g_\alpha^{1/2}} - \frac{g_\alpha^{1/2}}{\lambda_\alpha}\right) \qquad (50)$$

where ν is the number density of network chains and L is the number of slip-links per network chain.

The elastic free energy of the deformed network can be obtained by integrating the stress, eq 50, over λ_α. The general solution of differential equations (25) and (50) has the form

$$F^{el}_{st}(\lambda) = F^{el}_{ph}(\lambda) + \frac{\nu kT}{2}L\sum_{\alpha}\left(\frac{\lambda_\alpha}{g_\alpha^{1/2}} + \frac{g_\alpha^{1/2}}{\lambda_\alpha}\right) - \nu TS\{g_\alpha\} \qquad (51)$$

where we added the contribution of the phantom network, eq 26, and g_α should be found from the minimum of the rhs of eq 51 with respect to g_α under the condition $g_x + g_y + g_z = 3$.

The function $S\{g_\alpha\}$ has the meaning of the entropy of the additional degrees of freedom corresponding to different allowed positions of slip-links along the chains. This entropy corresponds to the diffusion of the stored length "defects" along the contour of the tube in the tube length fluctuation model.[27]

To estimate the entropy $S\{g_\alpha\}$ of the slip-tube model, we note that, on average, the tube changes its direction at each slip-link. Therefore, we can consider a tube which can only be oriented along the three major directions of the deformation. The average number of tube sections directed along each of these three directions is $L_x = L_y = L_z = L/3$. The entropy of an ideal one-dimensional gas of slip-links that cannot pass through each other is

$$S\{g_\alpha\} = k\sum_{\alpha} L_\alpha \ln\left(\frac{N_\alpha}{L_\alpha}\right) = \frac{kL}{3}\ln\left[\left(\frac{N}{L}\right)^3\prod_{\alpha} g_\alpha\right] \qquad (52)$$

The parameters g_α can be found from the minimum of the free energy, eq 51, with respect to g_α. Taking the condition $g_x + g_y + g_z = 3$ into account by the Lagrange multiplier method, we find the analytical solution for small deformation $|\lambda_\alpha - 1| \ll 1$:

$$g_\alpha - 1 = \frac{6}{7}\left(\lambda_\alpha - \frac{1}{3}\sum_{\beta}\lambda_\beta\right) \qquad (53)$$

As follows from eq 53, an isotropic swelling does not lead to chain slippage along the tube. For small deformations of an incompressible network, eq 53 becomes $g_\alpha - 1 = 6(\lambda_\alpha - 1)/7$. Substituting it into eq 50, we find the elastic stress

$$\sigma^{el}_{\alpha\beta} = 2(G_c + G_e)(\lambda_\alpha - 1)\delta_{\alpha\beta} \qquad (54)$$

where the phantom and entanglement contributions to the elastic modulus of the network are

$$G_c = \nu kT\left(1 - \frac{2}{\phi}\right), \quad G_e = \frac{4}{7}\nu kTL \qquad (55)$$

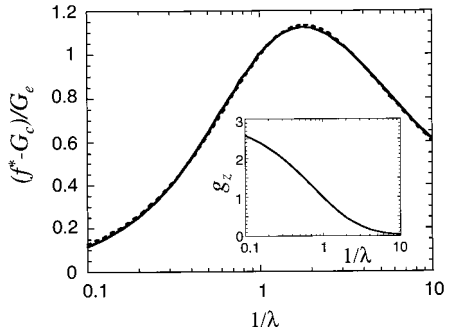

Figure 8. Comparison of the exact solution of the slip-tube model (solid line) for the entanglement part of the Mooney ratio with the approximate expression given in eq 59 (dashed line). The redistribution parameter g_z of the stored length between different directions of deformation decreases monotonically with reciprocal deformation $1/\lambda$ as shown in the insert.

Substituting eq 54 into the definition of the Mooney ratio (eq 33), we find

$$f^*(1) = G_c + G_e \tag{56}$$

Note that this relation is of general applicability and does not rely on any details of entanglement model.

In the case of uniaxial deformation ($\lambda_x = \lambda_y = \lambda_z^{-1/2}$, $\lambda_z = \lambda$), we have $g_x = g_y = (3 - g_z)/2$. Minimizing the free energy, eq 51, with respect to g_z, we find the following equation for the redistribution parameter g_z of chain length between different directions:

$$\frac{\lambda}{g_z^{3/2}} - \frac{1}{\lambda g_z^{1/2}} - \frac{1}{\lambda^{1/2}}\left(\frac{2}{3-g_z}\right)^{3/2} + \lambda^{1/2}\left(\frac{2}{3-g_z}\right)^{1/2} = \frac{4(g_z-1)}{g_z(3-g_z)} \tag{57}$$

The solution of this equation defines a universal function $g_z(\lambda)$, which is shown in the insert in Figure 8. For the undeformed network $\lambda = 1$, there is no redistribution of chain length between different directions and $g_z(1) = 1$. In the case of strongly compressed network, $\lambda \ll 1$, the redistribution parameter vanishes quadratically in λ as $g_z(\lambda) \approx 3.5\lambda^2$, and all of the chain length is stored only in the plane perpendicular to the direction of compression, $N_x = N_y \simeq N/2$. In the case of strong stretching, $\lambda \gg 1$, the chain is pulled out from perpendicular directions into the stretching one, and the parameter $g_z = 3N_z/N$ approaches 3 hyperbolically in λ as $g_z(\lambda) \approx 3 - 4.7/\lambda$. Substituting these limiting values ($g_z(0) = 0$ and $g_z(\infty) = 3$) into eq 50, one finds the asymptotic behavior of the entanglement part of the Mooney ratio, eq 33, in the two limits

$$f^*(\lambda^{-1}) \sim \begin{cases} \lambda^{-1} & \text{for } \lambda \gg 1 \\ \lambda^{1/2} & \text{for } \lambda \ll 1 \end{cases} \tag{58}$$

For any finite value of λ, eq 57 can be solved numerically for $g_z(\lambda)$ (see insert in Figure 8). Substituting this solution of $g_z(\lambda)$ into eq 50 and adding the contribution of the phantom network, eq 23, we find the exact solution for the stress of the slip-tube model. The results can be represented in the form of the Mooney ratio, eq 33. The normalized entanglement part ($f^*(\lambda^{-1}) - G_c)/G_e$ of the exact solution of the slip-tube model is shown as solid line in Figure 8. This exact solution is well approximated in the interval $0.1 < \lambda < 10$ by a simple analytical expression (dashed line in Figure 8).

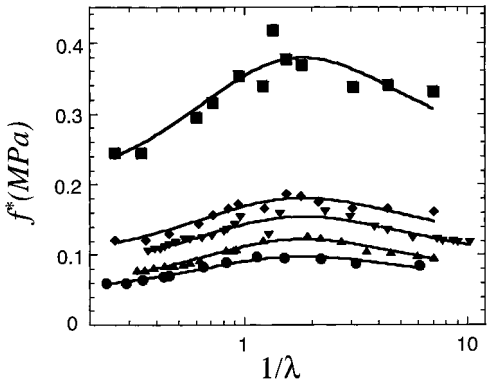

Figure 9. Mooney plot of the comparison of the experiments on uniaxial deformation with the slip-tube model (solid lines): (■, fitting parameters $G_c \simeq 1.77 \times 10^5$Pa and $G_e \simeq 1.77 \times 10^5$Pa, and ♦, $G_c \simeq 8.9 \times 10^4$Pa, $G_e \simeq 8.1 \times 10^4$Pa) natural rubber networks;[30] (▼, $G_c \simeq 6.9 \times 10^4$Pa, $G_e \simeq 7.5 \times 10^4$Pa, ▲, $G_c \simeq 4.4\times10^4$Pa, $G_e \simeq 6.8 \times 10^4$Pa,[29] and ●, $G_c \simeq 4.3 \times 10^4$Pa, $G_e \simeq 4.8 \times 10^4$Pa[20]) PDMS networks.

$$\frac{f^*(\lambda^{-1}) - G_c}{G_e} = \frac{1}{0.74\lambda + 0.61\lambda^{-1/2} - 0.35} \tag{59}$$

Note that this analytical appoximation (eq 59) of an exact soltion is consistent with eq 56. We would like to point out that there are no adjustable parameters in the theory besides the two physical moduli G_c and G_e. The three coefficients in eq 59 were chosen to obtain the best analytical approximation of the exact solution and are not adjustable parameters of the model (see Figure 8). Both exact numerical solution of the slip-tube model and its simple analytical approximation allow one to separate the phantom and entanglement contributions of the Mooney function $f^*(\lambda^{-1})$.

$$f^*(\lambda^{-1}) = G_c + \frac{G_e}{0.74\lambda + 0.61\lambda^{-1/2} - 0.35} \tag{60}$$

The network deformation factor λ enters only in the entanglement part of expression 60. This enables one to analyze the experimental data in the form of the universal plot as will be demonstrated in section 5 below.

5. Universal Plot

As can be seen from Figure 5, the prediction of the slip-tube model (solid line is a fit by eq 60) is in very good agreement with uniaxial deformation experiments on poly(dimethylsiloxane) (PDMS) networks (open circles).[20] Note that our slip-tube model captures both the shape and the location of the peak in the Mooney plot (Figure 5) much better than the nonaffine tube model (dash−dotted line) and better than the diffuse-constraint model (dashed line).

Quantitative comparison between the nonaffine tube model and the experimental results on uniaxial extension of polybutadiene networks[28] was carried out in ref 6. We fit these data with our new slip-tube model and find an even better agreement. Unfortunately, this set of data covers a limited range of uniaxial elongations $0.75 \lesssim \lambda \lesssim 0.95$. Experimental data covering almost 2 decades of uniaxial deformations of PDMS networks and natural rubber[20,29,30] are compared with the slip-tube mode (eq 60) in Figure 9. The models captures the main

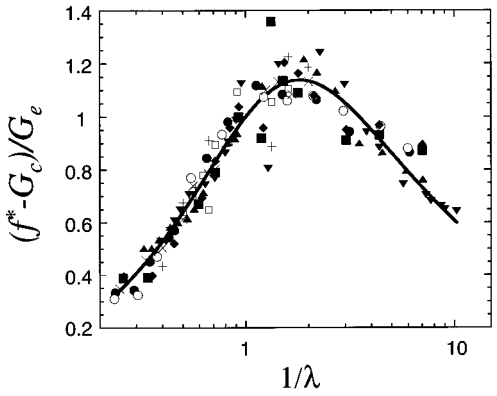

Figure 10. Universal plot for the reduced stress in uniaxially deformed networks. Symbols of the experimental data sets are the same as in Figures 5 and 9. Three additional data sets are from computer simulations[31] of end-linked networks with $N = 35$ monomers (□), $N = 100$ (+), and $N = 350$ (×).

features of experimental data including the position and the width of the peak of the Mooney ratio.

The approximate solution of the slip-tube model (eq 60) suggests a useful comparison between the theory and experimental data in the form of a universal plot. The approximate solution consists of two parts: the modulus of the phantom network, G_c, and the universal entanglement function. Universal plot can be obtained by subtracting the phantom modulus G_c from the Mooney function f^* and dividing the difference by the entanglement modulus G_e. The best collapse of all the data to the universal curve gives a pair of adjustable parameters G_c and G_e for each network. Variations of entanglement moduli from sample to sample could be related to different amounts of trapped entanglements and network imperfections.

The result of this procedure is shown in Figure 10. Besides the five sets of data from Figure 8, we added an additional set of data for PDMS networks[20] presented in Figure 5. In addition to these six experimental data sets, we included three data sets obtained by computer simulations of uniaxially deformed networks with strands containing $N = 35$ monomers (□), $N = 100$ (+), and $N = 350$ (×).[31] All nine data sets consisting of six experimental and three numerical sets collapse very well onto a single theoretical universal plot of eq 59 (solid line in Figure 10). Deviations from this universal curve are smaller than fluctuations within each individual set of data. Results of recent computer simulations of Chen, Cohen, and Escobedo[32] also agree well with the universal curve. The excellent agreement between the theory, experiments, and simulations demonstrates that the slip-tube model captures the essential physics of rubber elasticity.

6. Conclusions

In the present paper, we have developed a new molecular model of rubber elasticity. This model incorporates the main successful ideas of several classical theories of polymer networks:

1. Affine Network Model. The main idea of this model is that macroscopic deformations of polymer networks are transmitted to individual chains through the affinely deformed *nonfluctuating elastic background*. In the simple affine network model, the ends of the individual chains are permanently attached to this elastic background; see Figure 1.

2. Phantom Network Model. This model takes into account the fact that junctions of network chains are not fixed in space but fluctuate around some average positions. Macroscopic deformations are not transmitted directly from the elastic background to these network chains but rather through a softer potential that can be represented by *effective chains*. Therefore, the multichain phantom network model is equivalent to the affine model with a single *combined chain* consisting of one network strand and two effective chains connecting its ends to the elastic nonfluctuating background; see Figure 2.

3. Constrained-Junction Model. The effect of topological interactions between neighboring network chains can be represented by a constraining potential acting on some monomers of these chains. In the constrained-junction model this confining potential acts only on junction points and can be modeled by additional *virtual chains* connecting these junction points to the nonfluctuating elastic background; see Figure 3. A very important concept introduced in the constraint-junction model is that the confining potential changes with the network deformation. Therefore, the *fluctuations of these virtual chains change affinely* with the network deformation; see eq 27.

4. Edwards Tube Model. Topological constraints of neighboring chains are imposed not only on junctions but all along the contour of the network strand. In the Edwards tube model, these topological constraints are represented by the topological potential acting on all monomers of the network. This potential restricts fluctuations of network monomers to the confining tube and can be represented by virtual chains connecting network monomers to the elastic nonfluctuating background; see Figure 6.

5. Nonaffine Tube Model. This model combines the main ideas of the constraint-junction and the Edwards tube models. As in the Edwards tube model, the virtual chains are connecting many monomers of the network strand to the nonfluctuating elastic background. As in the constrained-junction model, the points of attachments of the virtual chains to the nonfluctuating elastic background are randomly scattered in space to guarantee the Gaussian statistics of network chains in the preparation conditions. As in the constrained-junction model, fluctuations of virtual chains change affinely with network deformations. In Appendix C, we demonstrate that this is the only possible assumption consistent with the microscopic definition of the stress tensor.

We build upon all the above ideas and introduce the new **Slip-Tube Model.** In this model, the junction points between network chains and virtual chains are replaced by *slip-links* attached to fluctuating ends of virtual chains. These slip-links are allowed to slide along the contour of the network chains but are not allowed to pass through each other (Figure 7). This model accounts for the redistribution of stored length along the confining tube.

The predictions of the slip-tube model are in very good agreement with the experimental data on uniaxial deformation of polybutadiene, PDMS, and natural rubber networks, as well as with numerical simulations. In agreement with predictions of the slip-tube model, six different sets of data for PDMS and natural rubber networks and three data sets from computer simulations collapse onto a single universal curve. A more quantitative comparison between the molecular parameters of

the slip-tube model and experiments requires a more systematic study of well-characterized polymer networks. We hope that this study will be carried out in the near future. In addition, a detailed comparison of the predictions of the slip-tube model with specific parameters of computer simulations of deformed polymer networks will allow further tests and refinements of our model.

Acknowledgment. M.R. acknowledges financial support of the National Science Foundation under Grants DMR-0102267, ECS-0103307, and CHE-9876674, as well as of the donors of the Petroleum Research Fund, administered by the American Chemical Society under Grant #37018-AC-7.

Appendix A. Index of Notations

$\langle ... \rangle$	averaging over thermal fluctuations
$\overline{...}$	averaging over all network chains
a	tube diameter of the Edwards tube model, eq 34
a_α	α-component of the tube diameter of the network deformed by factor λ_α
B	function defined in eq B5
b	monomer size
$b'_\alpha = b g_\alpha^{1/2}$	size of monomeric units consisting of g_α real monomers; see eq 48
$C(k_1, k_2)$	correlation function of the coordinates of attachment points of confining virtual chains on the Cayley tree; see eq D8
c	monomer concentration
D	function defined in eq B5
F	network free energy density; see eq 2
F_{af}^{el}	elastic free energy density of the affine network model, eq 6
F_{ch}^{el}	elastic free energy density of a Gaussian chain, eq 4
F_{cj}^{el}	elastic free energy density of the constrained-junction model, eq D20
F_{naf}^{el}	elastic free energy density of the nonaffine tube model, eqs 43 and 45
F_{ph}^{el}	elastic free energy density of the phantom network model, eq 26
F_{st}^{el}	elastic free energy density of the slip-tube model, eq 51
$f^*(\lambda^{-1})$	Mooney ratio; see eqs 33 and B1
$g_\alpha = N_\alpha / N_\alpha^0$	redistribution parameter of chain length along the axis α; see eq 48
G_c	phantom modulus
G_e	entanglement modulus
$i_k = 1, ..., \phi - 1$	index of the branch of the kth generation of the root Cayley tree
$K(\lambda_\alpha) = \sigma_{\alpha\alpha}$	diagonal component of the stress for uniaxially deformed network; see eq B1
k	Boltzmann factor
L	total number of slip-links per network chain
L_α	number of tube segments per network chain directed along the axis α; see eq 52 (on average $L_\alpha = L/3$)
$m_\alpha = m^0 \lambda_\alpha^2/3$	number of monomers along the axis α of confining virtual chains in the network deformed by factor λ_α; see eq 27
m^0	number of monomers of confining virtual chains in undeformed network
$m(p)$	number of monomers along any axis of confining virtual chains in the nonaffine tube model for undeformed network (for the Edwards tube model it does not change upon deformation)
$m_\alpha(p) = m(p)\lambda_\alpha^2$	number of monomers of confining virtual chains along axis α in the nonaffine tube model for the network deformed by factor λ_α
N	number of monomers of the network chain
N_α^{aff}	number of monomers in the affine strand of the network chain; see eq 40
N_e	number of monomers between entanglements
$N_\alpha = g_\alpha N_\alpha^0$	number of chain monomers directed along major axis α of the network deformation
N_α^0	number of chain monomers directed along the axis α in undeformed network (on average $N_\alpha^0 = N/3$)
N_{ch}	total number of network chains
N_{cr}	total number of network cross-links
$N(k_1, k_2)$	total number of paths that begin and end at k_1th and k_2th generations of the left and right Cayley trees, respectively; see eq D7)
n	number of monomers of effective chains in the combined chain model for the phantom network, see eq 16)
n_α	number of monomers along axis α of effective chains in the combined chain model for the network deformed by factor λ_α; see eq 28
$n_\alpha^{\|\|}$	parameter introduced in eq 29
$P_N(\mathbf{R})$	end-to-end correlation function of Gaussian chain of N monomers, eq C2
p	number of monomers along any axis between neighboring points of attachments of confining virtual chains to the network chain
q	parameter introduced in eq D9
$\mathbf{R}$	end-to-end vector of network chain
$\mathbf{R}_k$	coordinate of kth cross-link in the network deformed by factor $\boldsymbol{\lambda}$
$\mathbf{R}'_k$	coordinate of kth cross-link in the network deformed by factor $\boldsymbol{\lambda}$ and $\mathbf{1} + \boldsymbol{\epsilon}$
R_α^{aff}	α-component of the affine length; see eq 41
$R_\alpha(s_\alpha)$	coordinate of s_αth monomer along axis α
s_α	index of the monomer directed along the axis α (in the lattice model)
$S\{g_\alpha\}$	entropy of slip-links in the slip-tube model; see eq 52
T	temperature
$\mathbf{X} = \mathbf{X}_2 - \mathbf{X}_1$	the vector between two points of attachments of confining virtual chains to the elastic nonfluctuating background in the network deformed by factor $\boldsymbol{\lambda}$; see eq 1
$\mathbf{X}'$	the vector between two points of attachments of confining virtual chains to the elastic nonfluctuating background in the network deformed by factors $\boldsymbol{\lambda}$ and $\mathbf{1} + \boldsymbol{\epsilon}$; see eq 3
$\mathbf{X}_i$	points of attachments of confining virtual chains to the elastic nonfluctuating background
$\mathbf{X}_i^0$	points of attachments of confining virtual chains to the elastic nonfluctuating background in undeformed network

$\mathbf{X}^{\mathrm{R,L}}_{i_1\ldots i_{k-1}}$	points of attachments of confining virtual chain on the kth generation of right (R) or left (L) root Cayley tree
$\mathbf{X}^{\mathrm{cR,L}}_{i_1\ldots i_{k-1}}$	points of attachments of effective chain on the kth generation of right (R) or left (L) root Cayley tree; see eq D4
z, z_α	parameters introduced in eqs B3 and 32
V	the volume of the network deformed by factors $\boldsymbol{\lambda}$
$V' = V \det(\mathbf{1} + \epsilon)$	the volume of the network deformed by factors $\boldsymbol{\lambda}$ and $\mathbf{1} + \epsilon$
$\alpha,\beta,\gamma = x, y, z$	components of the Cartesian coordinate system (major axes of network deformation)
$\delta_{\alpha\beta}$	Kronecker delta function
$\Delta\mathbf{R} = \mathbf{R} - \langle\mathbf{R}\rangle$	fluctuations of the end-to-end vector $\mathbf{R}$ of a network chain
ϵ	infinitesimal strain tensor with components $\{\epsilon_{\alpha\beta}\}$
$\epsilon_{\alpha\beta}$	component of the infinitesimal strain tensor ϵ
θ	fractional distance along the chain in the diffused-constraint model; see eqs B6 and B7
κ	parameter characterizing the strength of constraints in the constrained-junction model; see eq B5
$\kappa(\theta)$	function of the fractional distance θ in the diffused-constraint model; see eq B7
$\boldsymbol{\lambda}$	deformation vector with components $\{\lambda_\alpha\}$
λ_α	coefficient of network deformation along the major axis of deformation ($\alpha = x, y, z$)
$\lambda'_\alpha = \lambda_\alpha\, g_\alpha^{1/2}$	renormalized because of the slippage coefficient of network deformation along the α axis; see eq 49
$\mu = 2c/(\phi N)$	number density of cross-links
$\nu = c/N$	chain number density
Π	pressure; see eq 8
$\sigma_{\alpha\beta}$	component of the stress tensor $\boldsymbol{\sigma}$; see eq 2
$\sigma^{\mathrm{el}}_{\alpha\beta}$	component of the elastic stress tensor $\boldsymbol{\sigma}^{\mathrm{el}}$
ϕ	functionality of network cross-links

Appendix B. Summary of Models of Rubber Elasticity

The Mooney ratio, eq 33, has the form

$$f^*(\lambda^{-1}) = \frac{K(\lambda) - K(\lambda^{-1/2})}{\lambda^2 - \lambda^{-1}} \tag{B1}$$

where $K(\lambda)$ is the model dependent function:

Exact Solution of the Constrained-Junction Model

$$K(\lambda) = kT\nu(\lambda^2 - 1)\left(\frac{1-z}{1+z}\right)^2 \frac{1 + z^2(\phi - 1)}{1 - z^2(\phi - 1)} \tag{B2}$$

where

$$z = 2\Big/\left[\phi + \frac{N}{m^0\lambda^2} + \sqrt{\sqrt{\left(\phi - 2 + \frac{N}{m^0\lambda^2}\right)^2 + \frac{4N}{m^0\lambda^2}}}\right] \tag{B3}$$

Approximate Solution of the Constrained-Junction Model

$$K(\lambda) = kT\nu\lambda^2\left[1 - \frac{2}{\phi} + \frac{2}{\phi}\left(\frac{BB'}{1+B} + \frac{DD'}{1+D}\right)\right] \tag{B4}$$

where $B' \equiv \partial B/\partial\lambda^2$, $D' \equiv \partial D/\partial\lambda^2$, and

$$B = \frac{\kappa^2(\lambda^2 - 1)}{(\lambda^2 + \kappa)^2}, \quad D = \frac{B\lambda^2}{\kappa}, \quad \kappa = \frac{N}{m^0}\frac{\phi - 1}{\phi(\phi - 2)} \tag{B5}$$

Approximate Solution of the Diffused-Constraint Model

$$K(\lambda) = kT\nu\lambda^2\left[1 - \frac{2}{\phi} + \frac{2}{\phi}\int_0^1 d\theta\left(\frac{B(\theta)B'(\theta)}{1 + B(\theta)} + \frac{D(\theta)D'(\theta)}{1 + D(\theta)}\right)\right] \tag{B6}$$

where the functions $B(\theta)$ and $D(\theta)$ defined in eq B5 with the substitution of $\kappa(\theta)$ for the parameter κ:

$$\kappa(\theta) = \frac{N}{m^0}\frac{\phi - 1}{\phi(\phi - 2)}\left[1 + \frac{(\phi - 2)^2}{\phi - 1}\theta(1 - \theta)\right] \tag{B7}$$

Nonaffine Tube Model

$$K(\lambda) = kT\nu\left(1 - \frac{2}{\phi}\right)\lambda^2 + \frac{kTc}{N_{\mathrm{e}}}\left(\lambda - \frac{1}{\lambda}\right) \tag{B8}$$

Slip-Tube Model

$$f^*(\lambda^{-1}) = kT\nu\left(1 - \frac{2}{\phi}\right) + \frac{kTc}{N_{\mathrm{e}}}\frac{1}{0.74\lambda + 0.61\lambda^{-1/2} - 0.35} \tag{B9}$$

Appendix C. Derivation of the Stress Tensor

C.1. Phantom Network Model. The elastic contribution to the partition function of the phantom network model is

$$\mathrm{e}^{-F^{\mathrm{el}}_{\mathrm{ph}}/(k\mathrm{T})} = \prod_k \int_{V'} \mathrm{d}\mathbf{R}'_k \prod_{kl} P_N(\mathbf{R}'_l - \mathbf{R}'_k) \tag{C1}$$

where the product is over all network chains and P_N is the end-to-end correlation function of Gaussian chain of N monomers

$$P_N(\mathbf{R}) = \prod_\alpha \left(\frac{3}{2\pi N b^2}\right)^{1/2} \exp\left(-\frac{3R_\alpha{}^2}{2b^2N}\right) \tag{C2}$$

The integration in eq C1 is only over the coordinates $\{\mathbf{R}'_k\}$ of cross-links in the volume V' of the network. The chains are permanently attached to the surface at the boundary and points of attachments X'_α change affinely with the network deformation; see eq 3. It is convenient to introduce new integration variables $\mathbf{R}_k$ in eq C1, $\mathbf{R}'_k \rightarrow \mathbf{R}_k$, where by analogy with coordinates of the elastic background, eq 3, we have

$$R'_{k\alpha} = R_{k\alpha} + \sum_\beta \epsilon_{\alpha\beta} R_{k\beta} \tag{C3}$$

In these new variables the integration volume V does not depend on the strain tensor ϵ. Substituting eqs C2 and C3 into eq C1, we find

$$e^{-F^{el}_{ph}/(kT)} = (2\pi Nb^2/3)^{-N_{ch}/2}[\det(1+\epsilon)]^{N_{cr}} \prod_k \int_V d\mathbf{R}_k\, e^{-E\{\mathbf{R}_k\}/(kT)} \quad (C4)$$

where N_{ch} is the total number of network chains and the number of cross-links is N_{cr}. The energy of a given configuration $\{\mathbf{R}_k\}$ is

$$E\{\mathbf{R}_k\} = \frac{3kT}{2b^2N}\sum_{kl}\sum_{\alpha\beta}(\delta_{\alpha\beta} + 2\epsilon_{\alpha\beta} + \sum_\gamma \epsilon_{\alpha\gamma}\epsilon_{\beta\gamma})R_{kl\alpha}R_{kl\beta} \quad (C5)$$

Differentiating the elastic free energy of the phantom network, eq C4, with respect to the components of the strain tensor, eq 2, we arrive at eq 17 for the stress tensor of the phantom network.

C.2. Constrained Models. Consider a network in a shape of a rectangular box with undeformed dimensions l^0_x, l^0_y, l^0_z. If the network is deformed by factors $\boldsymbol{\lambda}$, its dimensions become $l_\alpha = \lambda_\alpha l^0_\alpha$ along axes α. It is convenient to use a generalization of the continuous Edwards model of the network[8] with the partition function

$$e^{-F(\lambda)/(kT)} = \int_{l_x l_y l_z} D\mathbf{R}\, e^{-[F^{el}_{ch}\{\mathbf{R}\} + U\{\mathbf{R}\}]/(kT)} \quad (C6)$$

Here $\mathbf{R}_i(s)$ is the coordinate of sth monomer of the chain i, and the sum over i is over all network chains. The elastic energy of network chains is

$$F^{el}_{ch}\{\mathbf{R}\} = \frac{3kT}{2b^2}\sum_i \int ds \left(\frac{\partial \mathbf{R}_i}{\partial s}\right)^2 \quad (C7)$$

and the energy of monomer interaction with excluded volume parameter v is given by

$$U\{\mathbf{R}\} = \frac{vkT}{2}\sum_{ij}\int ds\, ds'\, \delta(\mathbf{R}_i(s) - \mathbf{R}_j(s')) \quad (C8)$$

In contrast to the Edwards model, where the integration over $\mathbf{R}$ is restricted only by boundaries of the box, in eq C6 the integration is over the region in conformation space, allowed by topological restrictions.

Since λ enters into eq C6 only implicitly, through the boundary conditions, this expression cannot be directly applied to calculate the stress

$$\sigma_{\alpha\alpha} = \lambda_\alpha \frac{\partial F(\boldsymbol{\lambda})}{\partial \lambda_\alpha} \quad (C9)$$

To get explicit dependence of the free energy on $\boldsymbol{\lambda}$, we change variables $R_\alpha = \lambda_\alpha R^0_\alpha$ in the integral over $\mathbf{R}$ in eq C6 and get

$$e^{-F(\lambda)/(kT)} = (\lambda_x\lambda_y\lambda_z)^{N_{tot}}\int_{l_x{}^0 l_y{}^0 l_z{}^0} D\mathbf{R}^0 \times \exp\left[-\sum_\alpha \frac{3\lambda_\alpha{}^2}{2b^2}\sum_i \int ds \left(\frac{\partial R^0_{i\alpha}}{\partial s}\right)^2 - \frac{1}{\lambda_x\lambda_y\lambda_z}\frac{U\{\mathbf{R}^0\}}{kT}\right] \quad (C10)$$

The factor $(\lambda_x\lambda_y\lambda_z)^{N_{tot}}$ is the Jacobian of the transformation $\mathbf{R} \rightarrow \mathbf{R}^0$ and N_{tot} is the total number of monomers. In the derivation of eq C10, we used the equality

$$\delta(\mathbf{R}_i(s) - \mathbf{R}_j(s')) = \frac{1}{\lambda_x\lambda_y\lambda_z}\delta(\mathbf{R}^0_i(s) - \mathbf{R}^0_j(s')) \quad (C11)$$

Obviously, this affine transformation does not change the topologically allowed region. Since the boundary conditions in eq C10 do not depend on λ, after substitution of eq C10 into eq C9 we have to differentiate only the integrand in eq C10. Substituting $R^0_\alpha = R_\alpha/\lambda_\alpha$ in the resulting expression and using eq C11, we reproduce the well-known Edwards expression for the stress of the network[15]

$$\sigma_{\alpha\alpha} = \sum_i \frac{3kT}{b^2}\int ds \left\langle\left(\frac{\partial R_{i\alpha}}{\partial s}\right)^2\right\rangle - N_{tot}kT - \langle U\{\mathbf{R}\}\rangle \quad (C12)$$

Here, the averaging is only over the topologically allowed region with the weight defined in eq C6. As claimed in ref 15, the factors NkT and $\langle U\{\mathbf{R}\}\rangle$ can be dropped from eq C12 for the incompressible network, since they only lead to isotropic renormalization of the pressure.

In this paper, we model topological restrictions by anisotropic virtual chains of yet unknown number m_α of monomers. Virtual chain k is attached to the network chain i at points s_k and is connected to an elastic nonfluctuating background at $\mathbf{X}_k$. This background deforms affinely with the network, $X_{k\alpha} = \lambda_\alpha X^0_{k\alpha}$. The free energy of such a network model is

$$e^{-F(\lambda)/(kT)} = \int_{l_x l_y l_z} D\mathbf{R}\, \exp(e^{-[F^{el}_{ch}\{\mathbf{R}\} + U\{\mathbf{R}\} + E_v\{\mathbf{R}\}]/(kT)}) \quad (C13)$$

where the integration is over all monomer coordinates $\mathbf{R}_i(s)$ inside the box with sizes $l_x l_y l_z$ occupied by the network (no restrictions due to network topology, as in eq C6). $E_v\{\mathbf{R}\}$ is the energy of virtual chains

$$E_v\{\mathbf{R}\} = kT\sum_k\sum_\alpha \frac{1}{2b^2 m_\alpha}[R_{i\alpha}(s_k) - X_{k\alpha}]^2 \quad (C14)$$

In the case of a nonaffine tube model, the positions of attachment points of virtual chains $\{s_k\}$ along the network chains are fixed. In the case of our new slip-tube model the elastic energy $F^{el}_{ch}\{\mathbf{R}\}$ of chains is given by eq 46, and one has to take additional integration of the partition function given by eq C13 over $\{s_k\}$ under the condition ... $< s_k < s_{k+1} <$ .... Let us find m_α from the condition that eqs C9 and C13 should reproduce exact Edwards expression for the stress, eq C12.

Changing variables, $R_\alpha = \lambda_\alpha R^0_\alpha$ in eq C13, we get

$$e^{-F(\lambda)/(kT)} = \int_{l_x{}^0 l_y{}^0 l_z{}^0} D\mathbf{R}^0 \times \exp\left\{-\sum_\alpha \frac{3\lambda_\alpha{}^2}{2b^2}\sum_i \int ds \left(\frac{\partial R^0_{i\alpha}}{\partial s}\right)^2 - \frac{1}{\lambda_x\lambda_y\lambda_z}\frac{U\{\mathbf{R}^0\}}{kT} - \sum_k\sum_\alpha \frac{\lambda_\alpha{}^2}{2b^2 m_\alpha}[R_{i\alpha}(s_k) - X_{k\alpha}]^2\right\} \quad (C15)$$

Substituting this expression into eq C9, we find

$$\sigma_{\alpha\alpha} = \sum_i \frac{3kT}{b^2} \int ds \left\langle \left(\frac{\partial R_{i\alpha}}{\partial s}\right)^2 \right\rangle - N_{tot}kT - \langle U\{\mathbf{R}\}\rangle + \frac{kT}{2b^2}\lambda_\alpha \frac{\partial}{\partial \lambda_\alpha}\left(\frac{\lambda_\alpha^2}{m_\alpha}\right) \sum_k \langle [R_{i\alpha}(s_k) - X_{k\alpha}]^2 \rangle \quad \text{(C16)}$$

Comparing eqs C12 and C16, we find the differential equation

$$\frac{\partial}{\partial \lambda_\alpha}\left(\frac{\lambda_\alpha^2}{m_\alpha}\right) = 0 \quad \text{(C17)}$$

which has a general solution

$$m_\alpha = \frac{1}{3} m^0 \lambda_\alpha^2 \quad \text{(C18)}$$

The constant of integration, m^0, cannot be derived from such consideration and should be considered as a phenomenological parameter. Inspection of eq C16 shows that if the number of monomers of virtual chains differs from that given by eq C18, there is an additional contribution to the stress from phantom virtual chains.[33] Because of the generality of our microscopic network model, eq C6, we do not see any physical reasons for such contribution.

Appendix D. Combined Chain for Constrained-Junction Network Model

A combined chain consists of a network chain and two combined virtual chains permanently attached to the nonfluctuating elastic background. To simplify notations we consider a one-dimensional problem, which corresponds to any of the principal directions of deformation, $\alpha = x, y, z$ and will drop the index α. Let us calculate the number of monomers n and the positions of attachment points X^{cR} and X^{cL} of right (R) and left (L) effective chains. The chains can be considered as a branched polymer on a Cayley tree with all of its cross-links connected through the confining virtual chains of $m = m^0\lambda^2/3$ monomers (eq 27) to the nonfluctuating background. As shown in Figure 11, the right effective chain can be considered as the result of the parallel connection of one confining virtual chain to $\phi - 1$ chains of $N/3 + n$ monomers. The end of the virtual chain is attached to the elastic background at position λX^R, and each of $\phi - 1$ chains is attached to the background at points X_i^{cR} ($i = 1, ..., \phi - 1$). The elastic energy of such connection can be written as

$$\frac{kT}{2b^2}\frac{(x - \lambda X^R)^2}{m^0\lambda^2/3} + \sum_{i=1}^{\phi-1} \frac{kT}{2b^2}\frac{(x - X_i^{cR})^2}{N/3 + n} = \frac{kT}{2b^2}\frac{(x - X^{cR})^2}{n} + \text{const} \quad \text{(D1)}$$

where x is the current coordinate of the connection point and the constant term does not depend on x. Equating the quadratic terms on both sides of eq D1, we get the following expression for the number of monomers in the effective chain

$$\frac{1}{n} = \frac{3}{m^0\lambda^2} + \frac{\phi - 1}{N/3 + n} \quad \text{(D2)}$$

The solution of this quadratic equation is given in eq 28.

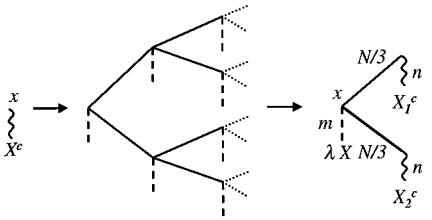

Figure 11. Effective chain can be considered as the result of a parallel connection of one confining virtual chain to $\phi - 1$ chains of $N/3 + n$ monomers.

Equating the terms linear in x on both sides of eq D1, we find

$$X^{cR} = [1 - z(\phi - 1)]\lambda X^R + z\sum_{i=1}^{\phi-1} X_i^{cR} \qquad z = n/(N/3 + n) \quad \text{(D3)}$$

The recurrence relation for the coordinates $X^{cR}_{i_1...i_{k-1}}$ of attachment points of the effective chain on kth generation of the root Cayley tree ($i_k = 1, ..., \phi - 1$ is the index of the branch of the kth generation) can be found by the analogy with eq D3:

$$X^{cR}_{i_1...i_{k-1}} = [1 - z(\phi - 1)]\lambda X^R_{i_1...i_{k-1}} + z\sum_{i_k=1}^{\phi-1} X^{cR}_{i_1...i_k} \quad \text{(D4)}$$

The solution of eqs D3 and D4 can be represented in the form of the infinite series

$$X^{cR} = \lambda[1 - z(\phi - 1)]\sum_{k=1}^{\infty} z^{k-1}\sum_{i_1...i_k} X^R_{i_1...i_k} \quad \text{(D5)}$$

where the internal summation is over all $(\phi - 1)^{k-1}$ branches on the kth generation of the root Cayley tree. Note that X^{cR} varies nonaffinely with the network deformation since the coefficient z depends on λ. An analogous expression for the coordinate of attachment point of the left effective chain X^{cL} is

$$X^{cL} = \lambda[1 - z(\phi - 1)]\sum_{k=1}^{\infty} z^{k-1}\sum_i X^L_{i_1...i_k} \quad \text{(D6)}$$

To calculate the correlation function $\overline{(X^{cR} - X^{cL})^2}$ we consider two symmetric paths on two connected Cayley trees, which start at k_1th and k_2th generations of the left tree and end at the corresponding generations k_1th and k_2th of the right tree; see Figure 11. The total length of the first path (the number of monomers which it passes through) is $(2k_1 - 1)N + 2m$ and that of the second path is $(2k_2 - 1)N/3 + 2m$. These paths can have a common part, which has a length $N/3 + 2kN/3 + 2m$ for the case if both paths coincide (with $k \equiv k_1 - 1 = k_2 - 1$) and the length $N/3 + 2kN/3$ otherwise (with $k < k_1$, k_2 and $k_1 \neq k_2$). According to eq D5, the correlation function under consideration can be written as

$$\overline{(X^{cR} - X^{cL})^2} = \lambda^2[1 - z(\phi - 1)]^2\sum_{k_1k_2} z^{2k_1+2k_2-2}N(k_1, k_2)C(k_1, k_2) \quad \text{(D7)}$$

The function

$$C(k_1, k_2) \equiv \overline{(X^{R}_{k1} - X^{L}_{k1})(X^{R}_{k2} - X^{L}_{k2})} \quad \text{(D8)}$$

is equal to b^2 times the length of the common path and $N(k_1, k_2)$ is the total number of the pair of paths which begin and end at k_1th and k_2th generations. The problem can be further simplified if we perform preliminary summation of contributions of two branches that are not common for both paths. Each of these branches gives the factor

$$q = z + z^2(\phi - 1) + z^3(\phi - 1)^2 + \ldots = z/[1 - z(\phi - 1)] \quad \text{(D9)}$$

Performing the remaining summation over k, we find

$$\overline{(X^{cR} - X^{cL})^2} = \lambda^2[1 - z(\phi - 1)]^2 \sum_{k=0}^{\infty} z^{2k}(\phi - 1)^k b^2 \times \frac{1}{3}\{(N + 2kN + 2m^0) + (N + 2kN)[2(\phi - 1)q + (\phi - 1)(\phi - 2)q^2]\} = \lambda^2 \frac{b^2}{3} \times \frac{N[1 + z^2(\phi - 1)] + 2m^0[1 - z(\phi - 1)]^2}{1 - z^2(\phi - 1)} \quad \text{(D10)}$$

This expression for the correlation function can be rewritten using $m^0 = 3m_\alpha/\lambda_\alpha^2$ from eq 27 and $N^0_\alpha = N/3$.

$$\overline{X_\alpha X_\beta} = \delta_{\alpha\beta}\frac{b^2}{3}\frac{N^0_\alpha \lambda_\alpha^2[1 + z^2(\phi - 1)] + 2m_\alpha[1 - z(\phi - 1)]^2}{1 - z^2(\phi - 1)} \quad \text{(D11)}$$

From eq D3 rewritten as

$$z_\alpha = \frac{n_\alpha}{N^0_\alpha + n_\alpha} \quad \text{(D12)}$$

we find

$$n_\alpha = N^0_\alpha \frac{z_\alpha}{1 - z_\alpha} \quad \text{(D13)}$$

and also

$$\frac{N^0_\alpha}{N^0_\alpha + 2n_\alpha} = \frac{1 - z_\alpha}{1 + z_\alpha} \quad \text{(D14)}$$

Combining eq D2 in the form

$$\frac{1}{n_\alpha} = \frac{1}{m_\alpha} + \frac{\phi - 1}{N^0_\alpha + n_\alpha} \quad \text{(D15)}$$

with eq D13, one can write

$$m_\alpha = N^0_\alpha \frac{z_\alpha}{1 - z_\alpha}\frac{1}{1 - z_\alpha(\phi - 1)} \quad \text{(D16)}$$

Substituting this expression into the correlation function (eq D11), we obtain

$$\overline{X_\alpha X_\beta} = \frac{b^2}{3}N^0_\alpha \delta_{\alpha\beta}\left[\lambda_\alpha{}^2\frac{1 + z^2(\phi - 1)}{1 - z^2(\phi - 1)} + 2\frac{z_\alpha}{1 - z_\alpha}\frac{1 - z(\phi - 1)}{1 - z^2(\phi - 1)}\right] \quad \text{(D17)}$$

This correlation function can be substituted into the expression for the elastic stress (eq 30)

$$\sigma^{el}_{\alpha\beta} = kT\nu\delta_{\alpha\beta}\left(\frac{N^0_\alpha}{N^0_\alpha + 2n_\alpha}\right)^2\left[\lambda_\alpha{}^2\frac{1 + z^2(\phi - 1)}{1 - z^2(\phi - 1)} + 2\frac{z_\alpha}{1 - z_\alpha}\frac{1 - z(\phi - 1)}{1 - z^2(\phi - 1)}\right] + kT\delta_{\alpha\beta}\left(\frac{2n_\alpha\nu}{N^0_\alpha + 2n_\alpha} - \frac{2\nu}{\phi}\right)$$

$$= kT\nu\delta_{\alpha\beta}\left(\frac{N^0_\alpha}{N^0_\alpha + 2n_\alpha}\right)^2\left[\lambda_\alpha{}^2\frac{1 + z^2(\phi - 1)}{1 - z^2(\phi - 1)} + 2\frac{z_\alpha}{1 - z_\alpha}\frac{1 - z(\phi - 1)}{1 - z^2(\phi - 1)}\right] + kT\nu\delta_{\alpha\beta}\left(1 - \frac{2}{\phi}\right) - kT\nu\delta_{\alpha\beta}\frac{N^0_\alpha}{N^0_\alpha + 2n_\alpha} \quad \text{(D18)}$$

The last step is the substitution of eq D14 into eq D18

$$\sigma^{el}_{\alpha\beta} = kT\delta_{\alpha\beta}\nu\left\{1 - \frac{2}{\phi} + \lambda_\alpha{}^2\left(\frac{1 - z_\alpha}{1 + z_\alpha}\right)^2\frac{1 + z^2(\phi - 1)}{1 - z^2(\phi - 1)} + 2\left(\frac{1 - z_\alpha}{1 + z_\alpha}\right)^2\frac{z_\alpha}{1 - z_\alpha}\frac{1 - z(\phi - 1)}{1 - z^2(\phi - 1)} - \frac{1 - z_\alpha}{1 + z_\alpha}\right\}$$

$$= kT\delta_{\alpha\beta}\nu\left\{1 - \frac{2}{\phi} + (\lambda_\alpha{}^2 - 1) \times \left(\frac{1 - z_\alpha}{1 + z_\alpha}\right)^2\frac{1 + z^2(\phi - 1)}{1 - z^2(\phi - 1)}\right\} \quad \text{(D19)}$$

The exact expression for the elastic free energy density F^{el}_{cj} of the constrained-junction model is obtained by integrating eq 25 with the stress given by eq D19:

$$F^{el}_{cj} = \frac{kT}{2}\sum_\alpha\left\{\nu\frac{N(\lambda_\alpha{}^2 - 1)}{N + 6n_\alpha} - \nu\ln\frac{N + 6n_\alpha}{(N + 3n_\alpha)^2} + \mu\ln\left[\frac{1}{3n_\alpha} + \frac{1}{N + 3n_\alpha}\right]\right\} \quad \text{(D20)}$$

References and Notes

(1) Kuhn, W. *J. Polym. Sci.* **1946**, *1*, 380. Wall, F. T.; Flory, P. J. *J. Chem. Phys.* **1951**, *19*, 1435. Flory, P. J. *Proc. R. Soc. Lond.* **1976**, A. *351*, 351.
(2) Landau, L. D.; Lifshitz, E. M. *Theory of Elasticity*, 3rd ed.; Pergamon: Oxford, England, 1986.
(3) James, H. M. *J. Chem. Phys.* **1947**, *15*, 651. James, H. M.; Guth, E. *J. Chem. Phys.* **1948**, *11*, 455.
(4) Flory, P. J. *Proc. R. Soc. London A* **1986**, *351*, 351.
(5) Higgs, P. G.; Ball, R. C. *J. Phys. (Paris)* **1988**, *49*, 1785.
(6) Rubinstein, M.; Panyukov, S. V. *Macromolecules* **1997**, *30*, 8036.
(7) Staverman, A. J. *Adv. Polym. Sci.* **1982**, *44*, 73.
(8) Edwards, S. F.; Vilgis, T. A. *Rep. Prog. Phys.* **1988**, *51*, 243.
(9) Ronca, G.; Allegra, G. *J. Chem. Phys.* **1975**, *63*, 4990.
(10) Flory, P. J. *J. Chem. Phys.* **1977**, *66*, 5120.
(11) Erman, B.; Flory, P. J. *J. Chem. Phys.* **1978**, *68*, 5363.

(12) Flory, P. J.; Erman, B. *Macromolecules* **1982**, *15*, 800.
(13) Erman, B.; Flory, P. J. *Macromolecules* **1982**, *15*, 806.
(14) Erman, B.; Mark, J. E. *Structure and Properties of Rubberlike Networks*; Oxford University Press: New York and Oxford, England, 1997.
(15) Doi, M.; Edwards, S. F. *The Theory of Polymer Dynamics*; Clarendon Press: Oxford, England, 1986.
(16) Erman, B.; Monnerie, L. *Macromolecules* **1989**, *22*, 3342.
(17) Erman, B.; Monnerie, L. *Macromolecules* **1992**, *25*, 4456.
(18) Mooney, M. *J. Appl. Phys.* **1948**, *19*, 434. Rivlin, R. S. *Philos. Trans. R. Soc. London Ser. A* **1948**, *A241*, 379.
(19) Kloczkowski, A.; Mark, J. E.; Erman, B. *Macromolecules* **1995**, *28*, 5089.
(20) Pak, H.; Flory, P. J. *J. Polym. Phys.* **1979**, *17*, 1845.
(21) Roland, C. M.; Mott, P. H. *Macromolecules* **1998**, *31*, 4033.
(22) Edwards, S. F. *Proc. Phys. Soc. (London)* **1967**, *92*, 9.
(23) Heinrich, G.; Straube, E. *Acta Polym.* **1983**, *34*, 589; **1984**, *35*, 115.
(24) Heinrich, G.; Straube, E. *Polym. Bull. (Berlin)* **1987**, *17*, 247; **1987**, *17*, 255.
(25) Ball, R. C.; Doi, M.; Edwards, S. F.; Warner, M. *Polymer* **1981**, *22*, 1010. Edwards, S. F.; Vilgis, T. A. *Polymer* **1986**, *27*, 483.
(26) de Gennes, P.-G. *Scaling Concepts in Polymer Physics*; Cornell University Press: Ithaca, NY, 1979.
(27) Doi, M. *J. Polym. Sci., Polym. Lett. Ed.* **1981**, *19*, 265; *J. Polym. Sci., Polym. Phys. Ed.* **1983**, *21*, 667.
(28) Dossin, L. M.; Graessley, W. W. *Macromolecules* **1979**, *12*, 123.
(29) Xu P.; Mark, J. E. *Rubber Chem. Technol.* **1990**, *63*, 276.
(30) Rivlin, R. S.; Saunders: D. W. *Phylos. Trans. R. Soc. London*, **1951**, *A 243*, 251.
(31) Grest, G. S.; Putz, M.; Everaers, R.; Kremer, K. *J. Non-Cryst. Solids* **2000**, *274*, 139.
(32) Chen, Z.; Cohen, C.; Escobedo, A. *Macromolecules* **2002**, *35*, 3296.
(33) Everaers, R. *Eur. Phys. J., B* **1998**, *4*, 341−350.

MA0203849